Stress-driven crystallization via shear-diffusion transformations in a metallic glass at very low temperatures

Yunwei Mao, Ju Li, Yu-Chieh Lo, Xiaofeng Qian, and Evan Ma

Phys. Rev. B **91**, 214103 — Published 5 June 2015

DOI: 10.1103/PhysRevB.91.214103

Stress-Driven Crystallization via Shear-Diffusion Transformations in a Metallic Glass at Very Low Temperatures

Yunwei Mao[a], Ju Li[b,a]*,Yu-Chieh Lo[b],Xiaofeng Qian[b], and Evan Ma[c,a]**,

[a] Center for Advancing Materials Performance from the Nanoscale, State Key Laboratory for Mechanical Behavior of Materials, Xi'an Jiaotong University, Xi'an 710049, China

[b] Department of Nuclear Science and Engineering and Department of Materials Science and Engineering, Massachusetts Institute of Technology, Cambridge, MA 02139

[c] Department of Materials Science and Engineering, Johns Hopkins University, Baltimore, MD 21218

*liju@mit.edu; **ema@jhu.edu

Abstract

At elevated temperatures, glasses crystallize via thermally activated diffusion. However, metallic glasses can also undergo deformation-induced crystallization at very low temperatures. Here we demonstrate the crystallization of $Al_{50}Fe_{50}$ metallic glasses under cyclic deformation at 50 K using molecular dynamics simulations, and reveal the underlying atomic-scale processes. We demonstrate that stress-driven non-affine atomic rearrangements, or shear diffusion transformation (SDT) events, lead to successive metabasin-to-metabasin transitions and long-range ordering. We also illustrate that the nucleation and growth of the crystal proceed via collective attachment of ordered clusters, advancing the amorphous/crystal interface in an intermittent manner. The cooperative nature of the step-like crystallization is attributed to the large activation volume of Eshelby transformations which generate as a byproduct non-affine "diffusive" atomic displacements that accumulate over loading cycles. The dual nature of "shear" (affine) and "diffusion" (non-affine) in low-temperature stress-driven SDT events thus unifies inelasticity with crystallization.

I. Introduction

Crystallization, including liquid-to-crystal transition (LCT) and glass-to-crystal transition, is an important process in materials physics. The mechanism of LCT in simple metals is now quite clear[1-3]: a series of monomolecular additions (condensations) to a droplet leads to crystal nucleation in the liquid, mediated by atomic attachments/detachments across the liquid/crystal interface[4]. In crystallization of glasses, most previous work has dealt with thermally-induced transitions upon heating of a glass to above its glass-transition temperature[5-7]. Nucleation and growth is again mediated by thermally activated diffusional hops of atoms at the glass/crystal interface.

In recent years, however, it has been proposed that metallic glasses (MGs) may also crystallize at very low temperatures (such as <77 K), if the MG is subjected to shear-dominated deformation[8-10]. This type of crystallization is not thermally induced, as the starting temperature is low, and deformation imposed causes little temperature rise[8, 11, 12]. This mechanical deformation-driven crystallization is in fact ubiquitous, in polymers[13], proteins and alloys[14]. But how the atoms reorganize under externally applied stresses to form crystals in the absence of temperature-induced atomic mobility, and what the differences are from thermal-diffusion mediated crystallization, remain largely unresolved. Low-temperature stress-driven *plasticity* of MGs is explained by Argon's shear transformation zone (STZ) model based on Eshelby's solution of sheared ellipsoids[15], including shear-banding which can be described as

spatially correlated STZ events[16, 17]. However crystallization must require non-affine, diffusive reorganization of atoms which seems to be outside of the STZ language.

Here we report a mechanistic study of the crystallization process in an $Al_{50}Fe_{50}$ MG, under cyclic loading in molecular dynamics(MD) simulations[12].A fatigue crack with appropriate geometry under cyclic loading was used, which would not generate a cross-sample large shear band[18] that may create temperature rise[19] and other complications[17, 20]. This geometry also gives rise to locations close to the crack tip, where the stress is amplified to accelerate the crystallization in local regions within the limited simulation time. Meanwhile, the stress gradient away from the crack ensures an elastic surrounding to conduct away the heat and keep the local crystallization zone under isothermal condition, and allows stable fatigue cycles to be accrued for easier observation of crystallization in small-scale simulations. Here crystallization is induced by the imposed stress at a very low temperature (50 K). The temperature was so low that no crystallization was possible from traditional mechanisms such as the diffusion-limited model based on transition rate theory or a collision-limited model[21]. It is the local accumulation of non-affine displacements with strain cycle that culminates in amorphous to crystal transition. In particular, we highlight cooperative behaviors unique to this form of crystal nucleation and growth in an amorphous matrix.

II. Simulation Details

MD simulations were conducted using LAMMPS[22],with atomic configurations displayed using AtomEye[23]. The atomic interactions in the $Al_{50}Fe_{50}$ alloy were

modeled using the embedded atom method potentials by Mendelev *et al.*[24]. A small glass sample consisting of 2000 atoms were prepared from a melting-and-quenching simulation of a random substitutional solid solution in a fcc lattice, which was heated from 300 to 3,000 K, equilibrated for 2 ns and then cooled down to 50 K, at an effective heating and cooling rate of 0.425 K/ps. The time step for integration was 2 fs. Pressure was maintained at zero during both the heating and cooling process. Periodic boundary condition was applied to all three directions. The final size of the small sample is ~ 4 nm × 4 nm × 2 nm. After that, a larger sample with final dimensions of ~ 59 nm × 74 nm × 2 nm was produced by duplicating the small sample along *x*- and *y*-axis. Then a crack of dimensions ~22 nm × 2 nm × 2 nm was introduced in the center of the sample. Fig. 1(a) shows the initial geometry of the sample, with dimensions of ~59 nm×74nm ×2nm and a crack-like notch with dimensions of 22nm × 2nm ×2nm.

The simulation was carried out as follows. We first applied a tensile strain of 3%(below the yield strain of ~5.6% at the strain rate of ~10^9/s), followed by cyclic loading (with a period of 20 ps and a strain amplitude of 1.8% along *y*-axis, see Fig. 1(b)). The strain along *z*-axis remains zero.

III. Results and Discussions

A. Deformation-induced crystallization

The final morphology after 355 cycles is displayed in Fig. 2(a). The atoms in different environments (characterized using the Honeycutt-Anderson method[25, 26]) are

highlighted using different colors, with blue, green, and maroon representing the bcc-, fcc-, and hcp-like atoms, respectively. Two relatively large crystals, C1 and C2, formed in the sample, in regions where the stresses are the highest. The directions of shear stress are marked with "τ" in Fig.2(a). The dense-packed planes of fcc/hcp/bcc are nearly aligned with the directions of the shear stress under this deformation-induced crystallization. This already reveals one difference from the case of scalar temperature-induced amorphous-to-crystal transition: the tensorial stress stimuli for crystallization lead to a preferred texture/directionality of the nucleated crystal, such that the nucleated crystals tend to have their crystallographic slip planes parallel to the local shear stress direction. The other basic difference from LCT is that a liquid state is at equilibrium, whereas our glass is out-of-equilibrium (non-ergodic) to start with, and with the application of large stress it potentially may step further away from equilibrium (rejuvenation). But instead, the cyclic stress here helps our simulation system to approach the true energy minimum, the crystalline state.

The potential energy of the whole system, including the atoms involved in crystallization and those that remained amorphous, is plotted as a function of cycle numbers in Fig.2(b). The corresponding rise of the fraction of crystallized atoms is shown in Fig.2(c). The crystallization process includes several stages: (1) an incubation period with almost constant potential energy (cycle<105). In this stage crystal-like atoms appear randomly but cannot be stabilized, with no net sustained fraction in Fig. 2(c); (2) a short period where the expected bcc phase (C1) nucleates (see the rapidly rising bcc atoms in Fig. 2(c)), sharply decreasing the potential energy(105< cycle< 125); (3) the fraction of bcc atoms continues to rise, together with a small fraction of fcc/hcp-like atoms(which emerge due to shear induced bcc-fcc transformation) in the growing C1 crystal. The growth of C1 crystal continuously

reduces the potential energy (125<cycle< 170). For cycle> 265, another bcc crystal C2 nucleates, similar to the case of C1.

B. Atomistic mechanism during the incubation period

During the incubation period, structural adjustments/relaxations result in some atoms with enhanced local order. The "ordered atoms" have a higher degree of short-to-medium range order relative to those in the glassy matrix; their high degree of rotational symmetry is quantified by the order parameters Q_6 and C_6[3, 27, 28], respectively.

Briefly, we characterize the local structure around particle *i* by a set of numbers

$$q_{lm}(i) = \frac{1}{N_i}\sum_{j\in N_i} Y_l^m(\hat{r_{ij}}) \qquad (1),$$

where $Y_l^m(\hat{r_{ij}})$ are spherical harmonics, $\hat{r_{ij}}$ is a unit vector in the direction of the bond between particle *i* and its neighbor *j*, and the sum runs over all N_i neighbors. A global bond parameter, such as Q_6, is obtained by computing $\bar{Q}_{lm}$, the average of $q_{lm}(i)$ over all particles, and then constructing a rotational invariant $Q_l(i)$.

$$Q_l(i) = \left[\frac{4\pi}{2l+1}\sum_{m=-l}^{l}|q_{lm}(i)|^2\right]^{1/2} \quad (2).$$

From the $\bar{q}_{lm}(i)$ we can, in the same way, construct an invariant $q_l(i)$ which measures the local bond order around particle *i*. The connection number of atom *i* is defined as

$$C_l(i) = \sum_{j\in N_i} H(S_{ij} - S_{thre}) \qquad (3),$$

where $H(x)$ is the step function. $S_{ij} = \sum_{m=-l}^{l}\tilde{q}_{lm}(i)\cdot\tilde{q}_{lm}^{\star}(i)$, and S_{thre} is a threshold

value set as 0.28 [3]. $\tilde{q}_{lm}(i)$ is defined as $\tilde{q}_{lm}(i) = q_{lm}(i)/|q_{lm}(i)|$.

Atoms with high C_6 ($C_6 > 10$) are called "ordered" atoms here. Fig. 3 shows the details of structural relaxations during the incubation stage for the atoms involved in crystals C1 and C2. Fig. 3(a)-(d) show the distribution of order parameter Q_6 in 1st, 60th, 110th and 270th cycle, respectively. Initially the order parameter is almost constant in the whole sample. With increasing cycles, certain areas highlighted by red and black frames, become more ordered and eventually result in nucleation of C1 and C2 (see the insert in (c) and (d)). Furthermore, Fig. 3(e)-(h) display the corresponding distributions of ordered atoms using connection number C_6 at the same cycle of (a)-(d). As the cycle goes on, the number of ordered atoms in active zones increases and these atoms form small clusters. The red and green frames highlight these changes. When these ordered clusters form, they are reshaped by the loading-induced stress/strain, some even grow up, leading to crystal nucleation (see the inset of (g) and (h), the light-blue atoms are crystal-like while the dark blue are deformation-induced ordered).

C. Atomistic mechanics during nucleation

Next, our focus is to uncover the details of the atomic-level processes that mediate crystallization. To this end, the C2 formation, which has a long incubation period (see Fig. 2) is analyzed in Fig. 4. An example is the 52 atoms supercluster in Fig.4. These distributed atoms then merge together later in a "jump" that nucleates the C2 crystal. In other words, clusters of ordered atoms cooperate to assemble into the nucleating crystal.

To confirm that this nucleation is temporally intermittent, we use a "distance matrix"(DM)[29, 30] to quantitatively assess the cooperative behavior of the 52-atom supercluster depicted in Fig. 4,

$$\Delta^2(t', t'') = \frac{1}{N}\sum_{i=1}^{N} |\boldsymbol{r}_i(t') - \boldsymbol{r}_i(t'')|^2, \qquad (1)$$

where $\boldsymbol{r}_i(t)$ is the position of particle i at time t.Fig.4(d) shows the DM of this supercluster as a function of two time arguments t'andt'', with darker compartments along the diagonal corresponding to the configurations that have "moved" only a small distance (DM) relative to one another. We observe that the dynamics of the supercluster is quite temporally intermittent: it stays in a local configuration space (i.e., a metabasin, defined as a set of configurations that make more frequent transitions between each other than with others[31, 32]) for a rather long period of time before it finds a pathway to jump into a new metabasin some distance (DM) away. A typical sojourn time within one metabasin is around 20-40 cycles, i.e., 400-800ps in our case. Fig. 4(e) shows$\delta^2(t, \theta)$, the particle averaged squared displacement (ASD) of the supercluster within a time interval θ. This function is defined as $\delta^2(t, \theta) =$

$\Delta^2(t-\frac{\theta}{2}, t+\frac{\theta}{2})$s [30]. Here we choose$\theta = 15$ cycles, which is sufficiently shorter than the α-relaxation time (in DM analysis, the typical size of dark squares along the diagonal is theα-relaxation time, marking the characteristic time-scale that a major configuration transformation happens[29, 30]). In our case, theα-relaxation time is 20-40 cycles but still considerably longer than the time period of microscopic vibrations. The ASD exhibits clear jumps corresponding to the hopping between metabasins in Fig. 4d. We conclude that the nucleation of crystal is due to the collaborative reorganization of many atoms (e.g., the 52 atoms in Fig. 4). Statistically, the supercluster involving atoms undergoing increasing ordering is observed to explore 3~6 metabasins before finally jumping into the crystal basin. The stress/strain serves as perturbations to trigger the metabasin-metabasin hops of this supercluster, relaxing the atoms involved into their more and more favorable configurations. This eventually ends with a collaborative action of all the atoms in and immediately next to the supercluster, directed/aligned by applied stresses, in establishing the crystal with translational symmetry. These features are quite different with that in LCT, where thermally activated diffusion of individual atoms is the dominant mediating process.

D. Atomistic mechanics during growth

The crystal nucleated then grows (the crystallization is preferentially in the nucleated regions where stresses are larger than in other areas). Fig.5 monitors the growth of the C1 crystal at various time intervals (in the 116th, 118th, 121st and 123rd cycle, respectively). Here the dark blue atoms are the "ordered atoms", again quantified by the order parameters Q_6 and C_6[3, 27, 28]. The atoms colored in light blue represent crystal atoms (Here we do not show the bcc/fcc/hcp atoms separately; all of them are

colored in light blue). We find that the growing crystal is always preceded by ordered atoms forming an encapsulating layer at the interface. This layer is formed by absorbing nearby small clusters of ordered atoms. The yellow and red lines in Fig. 5(a)-(d) highlight the advancement of one interface. From the 116th cycle to the 118th cycle, the interface marches forward rapidly (3 layers for 2 periods), but in the ensuing 118th-123rdcycles, the interface grows slowly (2 layers for 5 periods). This is an example indicating that the growth is also temporally intermittent, similar to the jerky basin hopping observed in the nucleation process (Fig. 4). Fig.5(e) shows the position(distance relative to its original location) of one particular interface as a typical example, at different times(cycles).The different colors rank the atomic order parameter Q_6 of the atoms. High values in the Q_6 order parameter represent ordered/crystal atoms (the green encapsulating layer/the growing crystal) while low values correspond to the glass matrix (blue region). Black arrows in Fig.5(e) mark the moments at which intermittent jumps occur, corresponding to the collective advancements of the interface. The crystal grows during some cycles (see the range of jump distances in Fig. 5(e)), and stops in some others. The probability of growth, along various directions, is presented in Fig.5(f), as a function of the wait time between the growth bursts. We use a power law, $P=fs^{-\Delta}\exp\left(-(s/t_0)^{\eta}\right)$ [33], to fit the data, where s is the wait time between two successive growth bursts, in Fig.3(e) and (f, Δ, t_0, η) are four fitted parameters. The fit gives f=0.4, Δ=0.2, t_0=140 ps (7 cycles), η=2.2.Note the cut-off $t_0$at 7 cycles, which represents that almost all crystal/glass interfaces will march within 7 cycles. This is at the same order of magnitude with that in experiment (in our experiments[12], within ~1000cycles, the crystal grows into a nanograin with a diameter of 30nm (~100 crystalline planes), then roughly 10-cycles is needed to advance the crystal/glass interface). The curve clearly shows that the

growth is intermittent and collective. The 140 ps (7 cycles) "cutoff" means that the wait time rarely exceeds 140 ps (7 cycles). Therefore 140 ps (7 cycles) is a characteristic time scale for this cooperative growth.

E. Differences between LCT and deformation-induced crystallization

To compare with the crystal growth in LCT, a 37×37×2nm $Al_{50}Fe_{50}$ sample of 200,000 atoms was cooled at a rate of 0.07K/ps. Two crystals nucleate at~1050K, followed by rapid growth. As seen in Fig.6, for crystal growth from liquid at this temperature, the fitted characteristic cut-off t_0 is only 12 ps. Moreover, the exponentηin the exponential tail of this distribution is 3.0, indicative of a faster process. The curve in Fig. 6 is now shifted to the left by one order of magnitude in time, and the interface moves almost continuously with a wait time of only a few ps. This can thus be perceived as a process via diffusive actions of *individual* atoms, just as in classical nucleation theory.

We next explain why the crystal formation requires cooperative actions in bursts. At a temperature far below T_g, thermal diffusion of atoms is suppressed, such that individual atoms do not have the mobility to search for low-energy locations by switching positions to join the incipient/growing crystal. Instead, small groups of atoms are agitated under tensorial stress to undergo shear-diffusion-transformations (SDT),

$$\mathbf{d}_{ji} \equiv \mathbf{d}_{ji}^0 \mathbf{J}_i + \mathbf{s}_{ji}, D_i^2 \equiv \min_{\mathbf{J}_i} \frac{1}{N_i} \sum_{j \in N_i} \left|\mathbf{s}_{ji}\right|^2, j \in N_i, \qquad (2)$$

where $j \in N_i$ are atom i's original nearest neighbors, and $\mathbf{d}_{ji}$ and $\mathbf{d}_{ji}^0$are the present and original distance vector between atom i and its original neighbor j.$\mathbf{J}_i$is a 3×3

matrix defined on each atom i, that is optimized for given sets of $\{\mathbf{d}_{ji}^0\}$ and $\{\mathbf{d}_{ji}\}$to minimizedthe local diffusion part D_i^2, constituting of non-affine displacement $\mathbf{s}_{ji}$ of each neighbor[19, 34]. In essence, equation (2) is an atomistic affine/non-affine decomposition, that seeks the best affine matrix connecting $\{\mathbf{d}_{ji}^0\} \rightarrow \{\mathbf{d}_{ji}\}$, but acknowledging that non-affine, or "diffusive" displacements may still exist as the residual displacements on top of that. While individual SDTs are akin to β relaxation events, the accumulation of the non-affine displacements$\mathbf{s}_{ji}$along the cyclic loading process by these SDT events plays the role of diffusion[12], to allow the atoms to develop more local order and gradually look for more comfortable configurations. Along the way towards the eventual crystal configurations, there are intermittent collective hopping events from metabasin to metabasin (akin to α relaxation, in steps), as discussed earlier. The collectivity of SDT events is characterized by the activation volume Ω, which is proportional to the number of atoms that simultaneously break their bonds at the saddle point[35] in a metabasin to metabasin transition. For purely temperature-driven LCT, the activation volume Ωinvolves one or a few atoms in simple metals. But for low-temperature, stress-driven SDT process discussed here, Ω involves many tens or even hundreds of atoms as illustrated by the MD data.

In equation (2) the non-negative D_i^2quantity is meant to be the parallel of mean squared displacement (MSD) in thermally driven diffusion, even though it is mainly stress driven. The defining characteristic of MSD in thermally driven diffusion is its linear growth with time. Here, D_i^2 accumulates approximately linearly with cycle number.With sufficient order accumulated collectively among the atoms involved in the group, the supercluster becomes "ready" to be pushed at the next moment (a bit more straining) into the crystal configuration, joining and expanding the crystal.

While the minimal "glass-to-crystal" distance, defined here to be the minimal non-affine displacement per atom necessary to re-order a disordered system into crystal, is as small as few angstroms[12], the energy barriers are too high at low temperatures if stress is not applied. A shear-dominant tensorial stress τ lowers the barrier Q significantly[36]. Indeed, the activation volume-tensor Ω is defined by how sensitive Q is to stress: $\Omega \equiv -\partial Q/\partial \tau$ [35], and a large activation volume means the barrier $Q(\tau)$ comes down quickly with increasing shear stress applied[17, 20, 35]. With Q lowered, "menu options" pop up to allow the local configurations to be nudged towards lower-energy valleys. As a result, along with the SDT-mediated ordering (e.g., rising Q_6) the glass undergoes the step-by-step metabasin-to-metabasin transitions to overcome the phase-space distance to crystal on the potential energy landscape. The patches of "ready-to-crystallize" atoms do not migrate in the absence of temperature-induced atomic mobility, so the advancing crystal has to wait for more of them to accumulate and link up right at the interface between the glass and the crystal (dark blue regions in Fig. 3).Through this stage, the precursors have incubated to the point that the barrier to reach the crystal becomes sufficiently small. Only then can they be collectively realigned to join the crystal by the stresses in ensuing deformation (readily falling into the crystal basin nearby). This precursor requirement extends the wait time to at least one order of magnitude longer than that in LCT (Fig. 6), making the interface advancement an intermittent process.

III. Conclusions

To recapitulate, our MD simulations reveal that in the absence of temperature-induced thermal diffusion of individual atoms[37], deformation-driven crystallization at very low temperatures is accomplished in cooperative steps. We find that both the crystal

nucleation and growth are temporally heterogeneous, exhibiting intermittent interface migration. For this new mode of crystallization, the highly cooperative nature is rooted in the larger activation volume Ω and the need to wait, i.e., to get ready (the glass in front of the crystal/glass interface need to incubate to accumulate local ordering to approach the crystal basin), which can only be accrued over a period of time (e.g., strain cycles here) for a collection of atoms through repeated non-affine displacements over a series of loading cycles. Such fatigue loading indeed makes the observation of low-T crystallization easier, since D_i^2 accrues approximately linearly with cycle number, while $\mathbf{J}_i$ oscillates but does not accumulate much; whereas in a monotonic loading to failure (fracture) setup, $\mathbf{J}_i$ accumulates but D_i^2 does not have enough time to accrue. Thus fatigue loading enhances the "diffusion"-to-"shear" (non-affine to affine) ratio of successive shear diffusion transformation events, making the low-T crystallization easier to simulate and study experimentally[12]. Crystallization via SDT is a low-temperature, stress-driven, larger-activation-volume process, when compared to LCT. SDT has the dual nature of "shear" and "diffusion", which is mathematically defined by an affine/non-affine decomposition of relative atomic displacements. As such, SDT is an extension of Argon and Eshelby's shear transformation concept[15, 16] which emphasized the affine (shape change) part of stress-driven processes[17, 20]. Previously, Delogu[38, 39] and Fujita *et.al.*[40] have also highlighted non-affine displacements. Such non-affine displacements, resulting in local diffusion, could change the initial atomic configuration of the system and eventually induce a disorder-order transition. With the diffusional contribution now properly defined, SDT can be used to explain not only the deformation strains but also the low-temperature crystallization in a metallic glass[8, 12, 15]. Finally, we note that solute partitioning is not observed in our experiment[12] or MD simulation, as the crystals

formed has the same chemical composition as the glass ("massive transformation"), so only short-range diffusion is necessary. In cases where a glass transforms to crystals (or even amorphous phases) with two or more different chemistries, solute partitioning and long-range diffusion have to occur. However, based on what we know about how D_i^2 accumulates with the number of SDT events, we predict that long-range diffusion and solute partitioning can also happen with stress-driven SDTs.

Acknowledgement

This work was supported in part by the 973 Program of China (2012CB619402). We also appreciate the support from the 111 Project of China (B06025). Both J.L. and E.M. benefited from an adjunct professorship at XJTU. Y.C.L., X.F.Q and J.L. acknowledge support by NSF DMR-1120901 and DMR-1240933. E.M. was supported at JHU by U.S.-DOE-BES, Division of Materials Sciences and Engineering, under Contract No. DE-FG02-09ER46056.

1 D. Turnbull, Contemporary Physics **10**, 473 (1969).
2 P. G. Debenedetti, *Metastable liquids: concepts and principles* (Princeton Univ Pr, 1996).
3 T. Kawasaki and H. Tanaka, Proceedings of the National Academy of Sciences **107**, 14036 (2010).
4 C. Angell, D. MacFarlane, and M. Oguni, Annals of the New York Academy of Sciences **484**, 241 (1986).
5 X. Liu, G. Chen, H. Hou, X. Hui, K. Yao, Z. Lu, and C. Liu, Acta Materialia **56**, 2760 (2008).
6 R. Kakkad, J. Smith, W. Lau, S. Fonash, and R. Kerns, Journal of applied physics **65**, 2069 (1989).
7 V. E. Borisenko and P. J. Hesketh, *Rapid thermal processing of semiconductors* (Plenum Pub Corp, 1997).
8 J. J. Kim, Y. Choi, S. Suresh, and A. Argon, Science **295**, 654 (2002).

[9] A. Kawashima, Z. YUQIAO, X. GUOQIANG, N. Nishiyama, and A. Inoue, Materials science & engineering. A, Structural materials: properties, microstructure and processing **528**, 391 (2010).
[10] F. Méar, B. Doisneau, A. Yavari, and A. Greer, Journal of Alloys and Compounds **483**, 256 (2009).
[11] B. Huang, R. Perez, P. Crawford, A. Sharif, S. Nutt, and E. Lavernia, Nanostructured materials **5**, 545 (1995).
[12] C.-C. Wang, Y.-W. Mao, Z.-W. Shan, M. Dao, J. Li, J. Sun, E. Ma, and S. Suresh, Proceedings of the National Academy of Sciences **110**, 19725 (2013).
[13] Y. Ogino, H. Fukushima, N. Takahashi, G. Matsuba, K. Nishida, and T. Kanaya, Macromolecules **39**, 7617 (2006).
[14] K. Kelton and A. L. Greer, *Nucleation in Condensed Matter: Applications in Materials and Biology* (A Pergamon Title, 2010).
[15] A. Argon, Acta metallurgica **27**, 47 (1979).
[16] C. A. Schuh, T. C. Hufnagel, and U. Ramamurty, Acta Materialia **55**, 4067 (2007).
[17] P. Zhao, J. Li, and Y. Wang, Acta Materialia **73**, 149 (2014).
[18] A. Greer, Y. Cheng, and E. Ma, Materials Science and Engineering: R: Reports **74**, 71 (2013).
[19] F. Shimizu, S. Ogata, and J. Li, Materials transactions **48**, 2923 (2007).
[20] P. Zhao, J. Li, and Y. Wang, International Journal of Plasticity **40**, 1 (2013).
[21] Y. Ashkenazy and R. Averback, Acta Materialia **58**, 524 (2010).
[22] S. Plimpton, Journal of Computational Physics **117**, 1 (1995).
[23] J. Li, Modelling and Simulation in Materials Science and Engineering **11**, 173 (2003).
[24] M. Mendelev, D. Srolovitz, G. Ackland, and S. Han, Journal of materials research **20**, 208 (2005).
[25] J. D. Honeycutt and H. C. Andersen, Journal of Physical Chemistry **91**, 4950 (1987).
[26] H. Tsuzuki, P. S. Branicio, and J. P. Rino, Computer physics communications **177**, 518 (2007).
[27] P. J. Steinhardt, D. R. Nelson, and M. Ronchetti, Physical Review B **28**, 784 (1983).
[28] P. R. Ten Wolde, M. J. Ruiz-Montero, and D. Frenkel, Physical review letters **75**, 2714 (1995).
[29] I. Ohmine, The Journal of Physical Chemistry **99**, 6767 (1995).
[30] G. Appignanesi, J. Rodriguez Fris, R. Montani, and W. Kob, Physical review letters **96**, 57801 (2006).
[31] A. Heuer, Journal of Physics: Condensed Matter **20**, 373101 (2008).
[32] J. C. Mauro, R. J. Loucks, and P. K. Gupta, The Journal of Physical Chemistry A **111**, 7957 (2007).
[33] F. F. Csikor, C. Motz, D. Weygand, M. Zaiser, and S. Zapperi, Science **318**, 251 (2007).
[34] M. Falk and J. Langer, Physical Review E **57**, 7192 (1998).
[35] J. Li, MRS bulletin **32**, 151 (2007).
[36] D. J. Lacks and M. J. Osborne, Physical review letters **93**, 255501 (2004).
[37] S. W. Nam, et al., Science **336**, 1561 (2012).
[38] F. Delogu, Intermetallics **19**, 86 (2011).
[39] F. Delogu, Materials Chemistry and Physics **126**, 152 (2011).
[40] T. Fujita, Z. Wang, Y. Liu, H. Sheng, W. Wang, and M. Chen, Acta Materialia **60**, 3741 (2012).

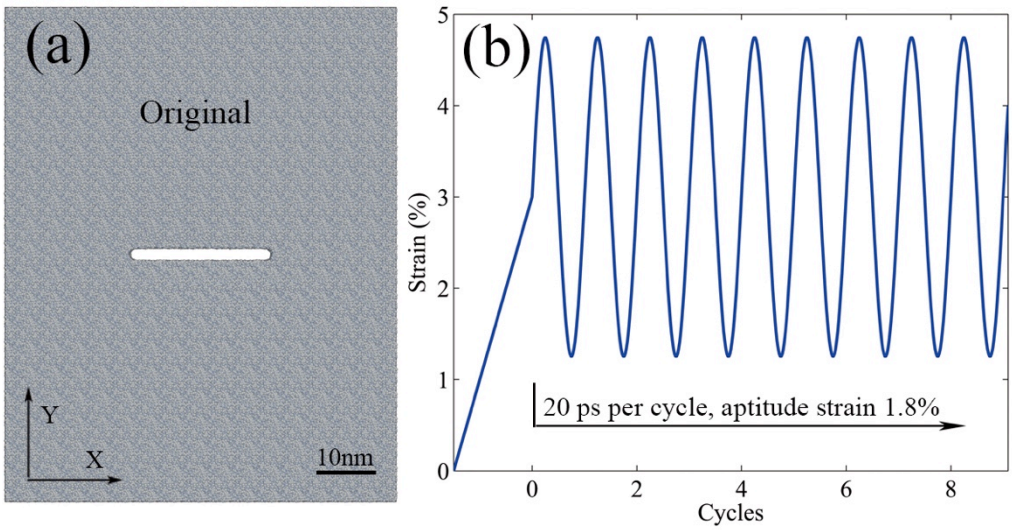

FIG 1. Molecular dynamics simulation setup. (a). Initial sample morphology with a crack. (b) Detailed loading function used in simulation See text for details.

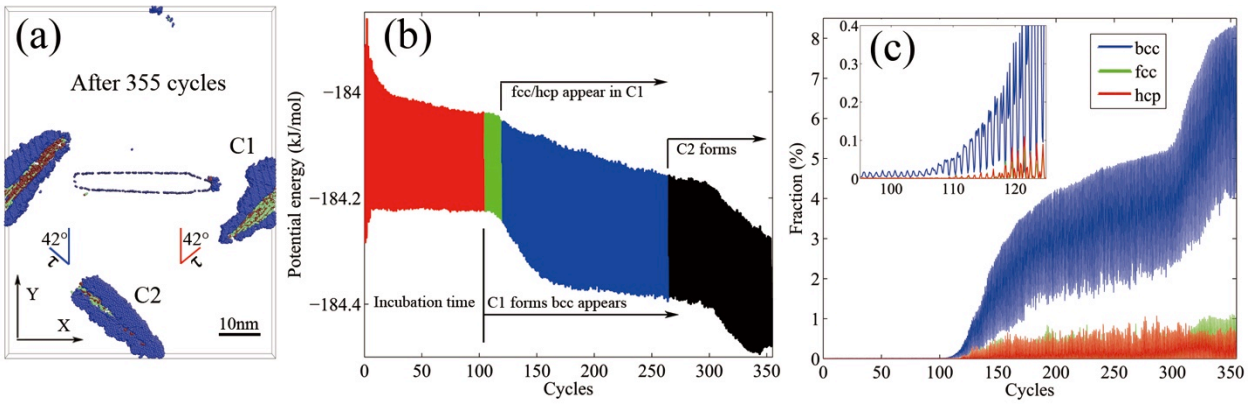

FIG 2. Molecular dynamics simulation of the cyclic-straining-induced crystallization in Al50Fe50 metallic glass. (a). Final morphology after 355 cycles. Two crystals (C1 and C2) form. (b) Potential energy versus loading cycles, showing obvious energy reduction during glass-crystal transition. (c). Ratio of crystal-like atoms versus cycles.

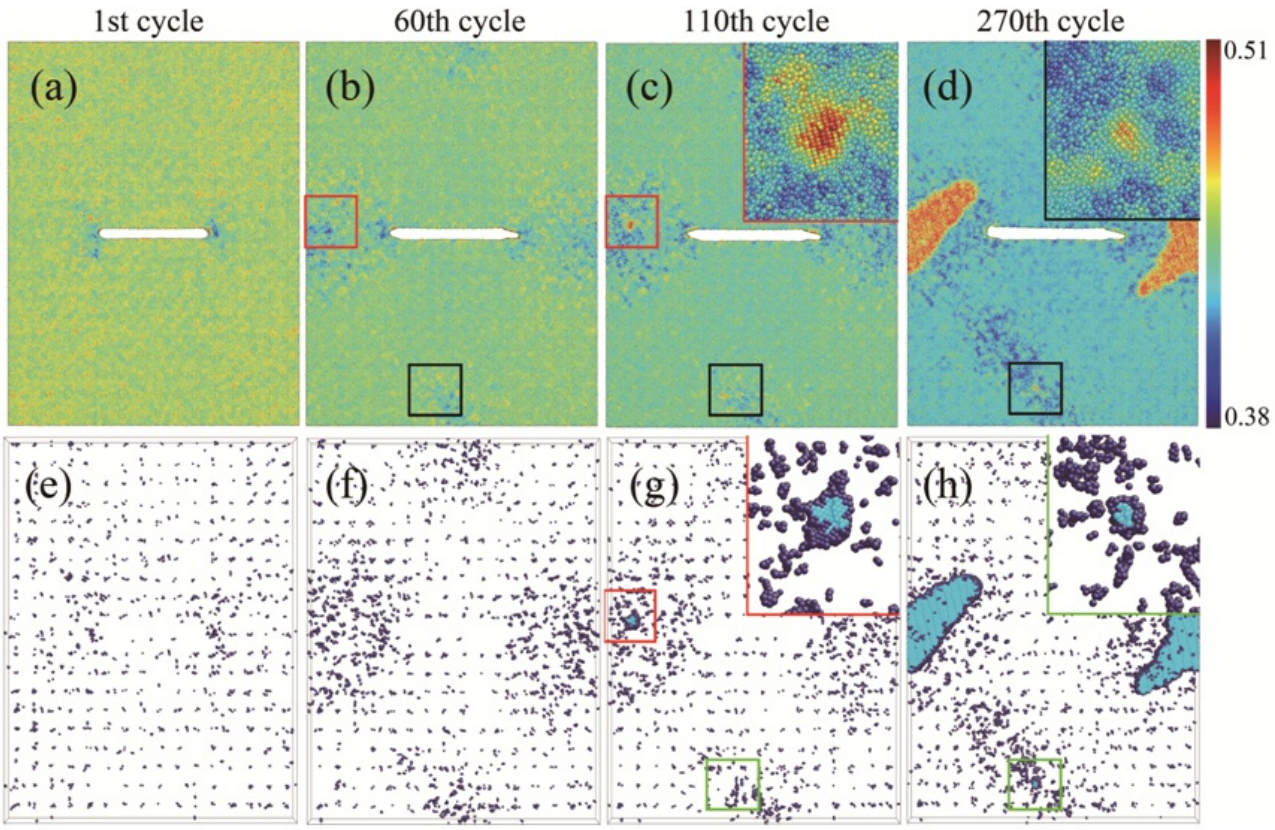

FIG 3. Structural relaxations within incubation time. (a)-(d) gives the distribution of order parameter Q6 in 1st, 60th,110th and 270th cycle. (e)-(h) gives the distribution of ordered atoms in corresponding cycles. The boxes in these figures highlight some active zones with a high content of ordered atoms, and close-up views are shown in the insets.

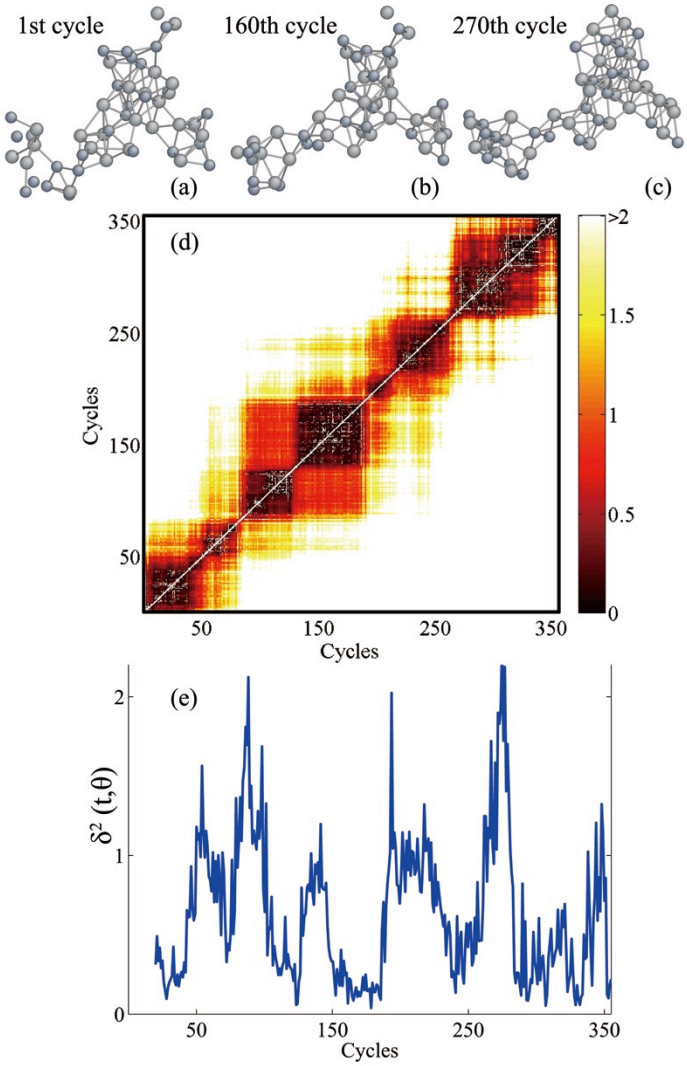

FIG 4. Atomic configuration during the formation of C2 and cooperative behavior of this cluster. The distributed 52 atoms in (a) are gradually assembled into more ordered packing (b through c) due to the accumulation of non-affine displacements under cyclic deformation. (d) shows DM for the cluster in (a). (e) ASD for the trajectory in (d). The value of θ $\delta^2(t, \theta)$is 15 periods.

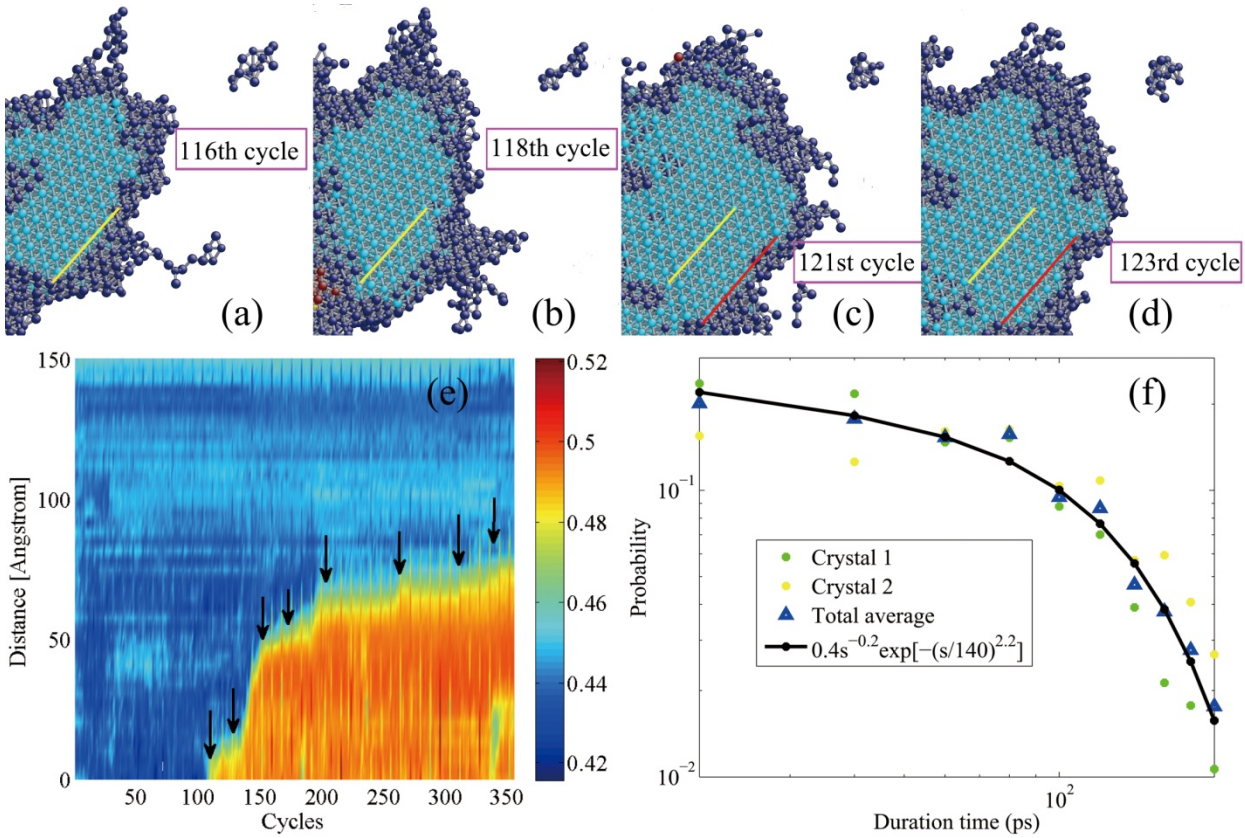

FIG 5. Cooperative behavior during the growth of crystal C1 in the MG matrix. (a)-(d) show the evolution of crystal/amorphous interface after 116, 118, 121 and 123 cycles. The ordered atoms (dark blue) transform into crystal and the corresponding interface moves outwards within 2 cycles as indicated by the position of the yellow line in (b), while the interface moves very little from (c) to (d). (e) A typical example showing the motion of the interface at different times (cycles). The different colors rank the atomic order parameter Q_6 of the atoms. High values in the Q_6 order parameter represent ordered/crystal-like atoms while low values correspond to the glass matrix (See section 3 in SI). Black arrows mark the intermittent jumps of the interface position, corresponding to the jerky and collective advancements of the interface. (f) Probability of the wait duration time for interface jump (in double-log plot). The data is fitted by a power law P=$0.4s^{-0.2}\exp\left(-(s/140)^{2.2}\right)$

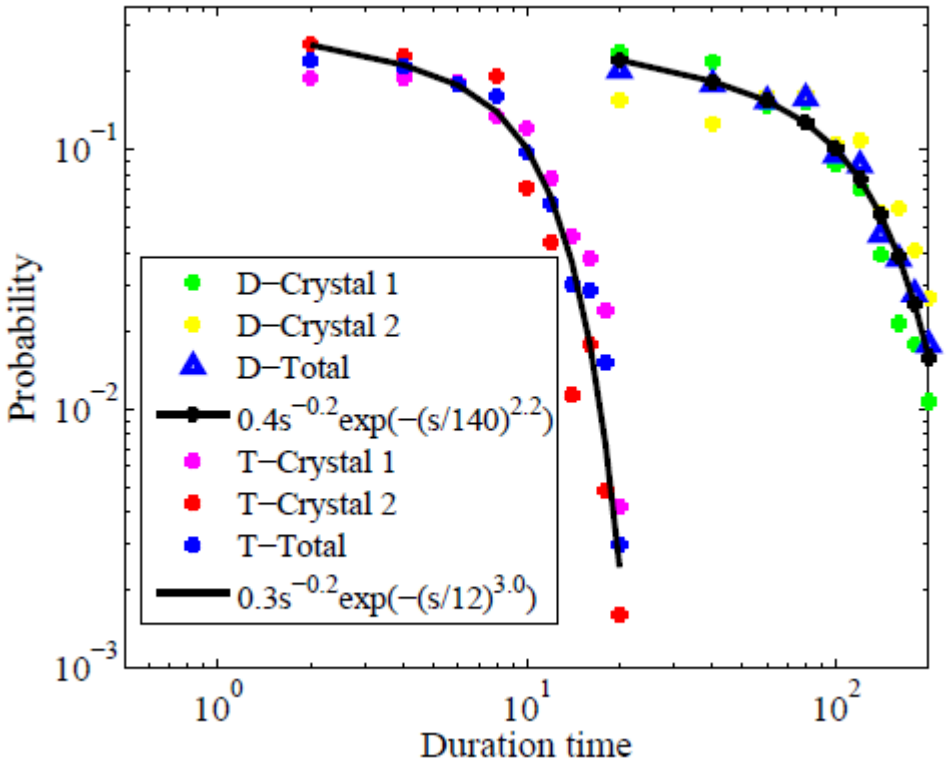

FIG 6.The advancement of crystal/amorphous interfaces, comparing temperature-induced (T-Crystal 1 and T-Crystal 2) versus deformation-induced (D-Crystal 1 and D-crystal 2) crystallization. D/T-total is for the sum of the two crystals. Black lines are guild to the eye.